SUPPORTING INFORMATION FOR:
Neutral one-dimensional metal chains consisting of alternating anionic and cationic rhodium complexes

Elina Laurila, Larisa Oresmaa, Jorma Hassinen, Pipsa Hirva and Matti Haukka*
[*] *Department of Chemistry, University of Eastern Finland, Joensuu Campus, P.O. Box 111, FI-80101 Joensuu, Finland.*
E-mail: matti.haukka@uef.fi

TABLE OF CONTENT

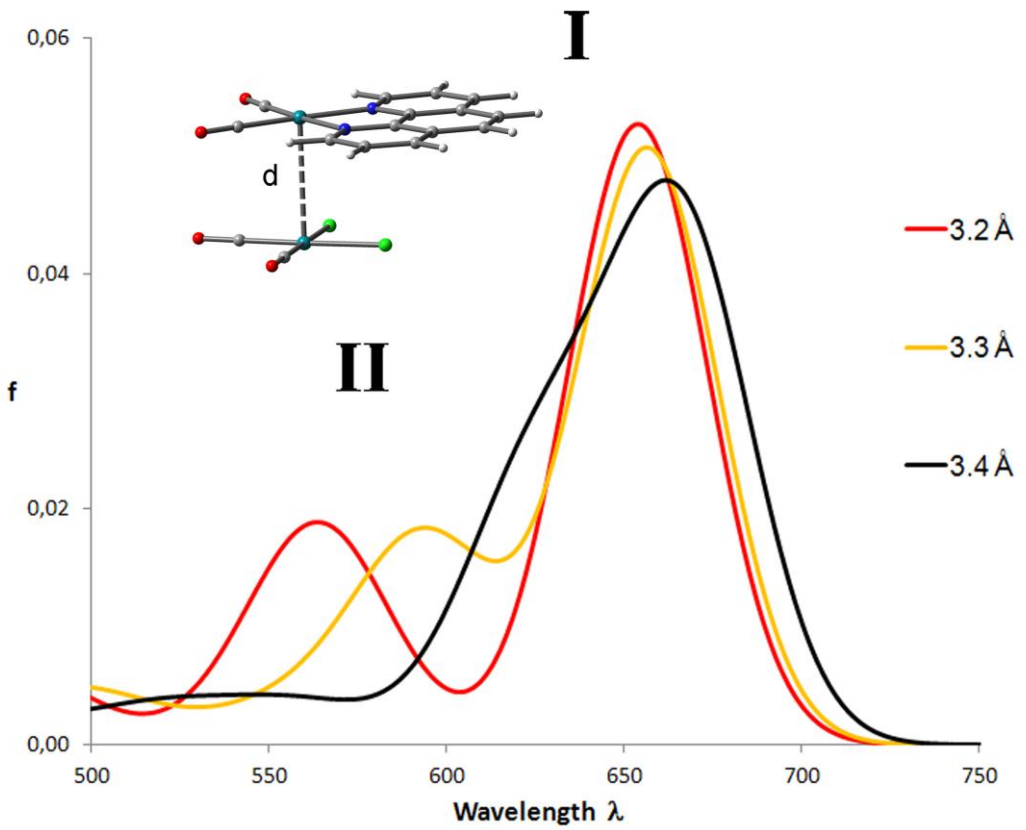

Figure S1. The effect of the Rh···Rh distance on the two lowest energy absorption signals of [Rh(1,10-phen)$(CO)_2$][Rh$(CO)_2Cl_2$] (**2**) based on TD-DFT calculations.

Table S1. The contribution of HOMO, HOMO-1 and LUMO orbitals on the lowest energy absorption signals of [Rh(2,2'-bpy)$(CO)_2$][Rh$(CO)_2Cl_2$] (**1**) and the properties of the electronic transitions based on TD-DFT calculations.

Rh···Rh (Å)	Signal	HOMO-LUMO %	HOMO-1-LUMO %	λ(nm)	f	HOMO-LUMO gap (eV)	HOMO-1-LUMO gap (eV)
3.2	I	87	4	666	0.0475	2.66	
	II	3	92	566	0.0201		3.03
3.3	I	85	6	669	0.0449	2.63	
	II	5	90	596	0.0223		2.90
3.4	I	79	13	679	0.0384	2.59	
	II	11	84	629	0.0276		2.77

λ: The absorption wavelength
f: The oscillator strength

Table S2 The contribution of HOMO, HOMO-1 and LUMO orbitals on the lowest energy absorption signals of [Rh(1,10-phen)$(CO)_2$][Rh$(CO)_2Cl_2$] (**2**) and the properties of the electronic transitions based on TD-DFT calculations.

Rh···Rh (Å)	Signal	HOMO-LUMO %	HOMO-1-LUMO %	λ(nm)	f	HOMO-LUMO gap (eV)	HOMO-1-LUMO gap (eV)
3.2	I	88	3	654	0.0527	2.68	
	II	2	93	565	0.0162		3.03
3.3	I	86	5	656	0.0506	2.65	
	II	4	91	594	0.0176		2.91
3.4	I	81	11	665	0.044	2.65	
	II	10	85	624	0.0223		2.91

λ: The absorption wavelength
f: The oscillator strength

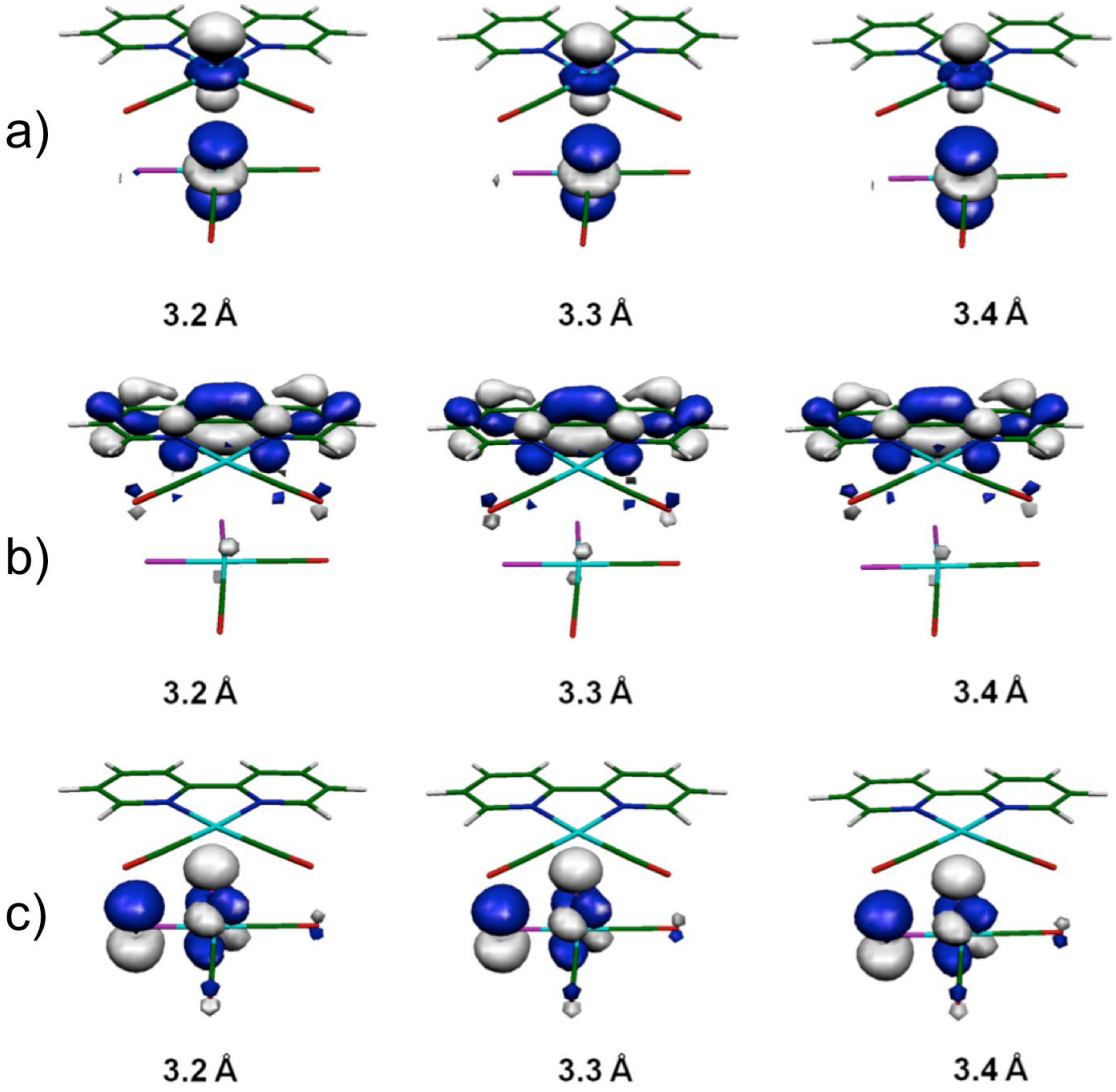

Figure S2. The HOMO (a), LUMO (b) and HOMO-1 (c) orbitals of $[Rh(2,2'\text{-bpy})(CO)_2][Rh(CO)_2Cl_2]$ (**1**) system at different rhodium···rhodium distances.

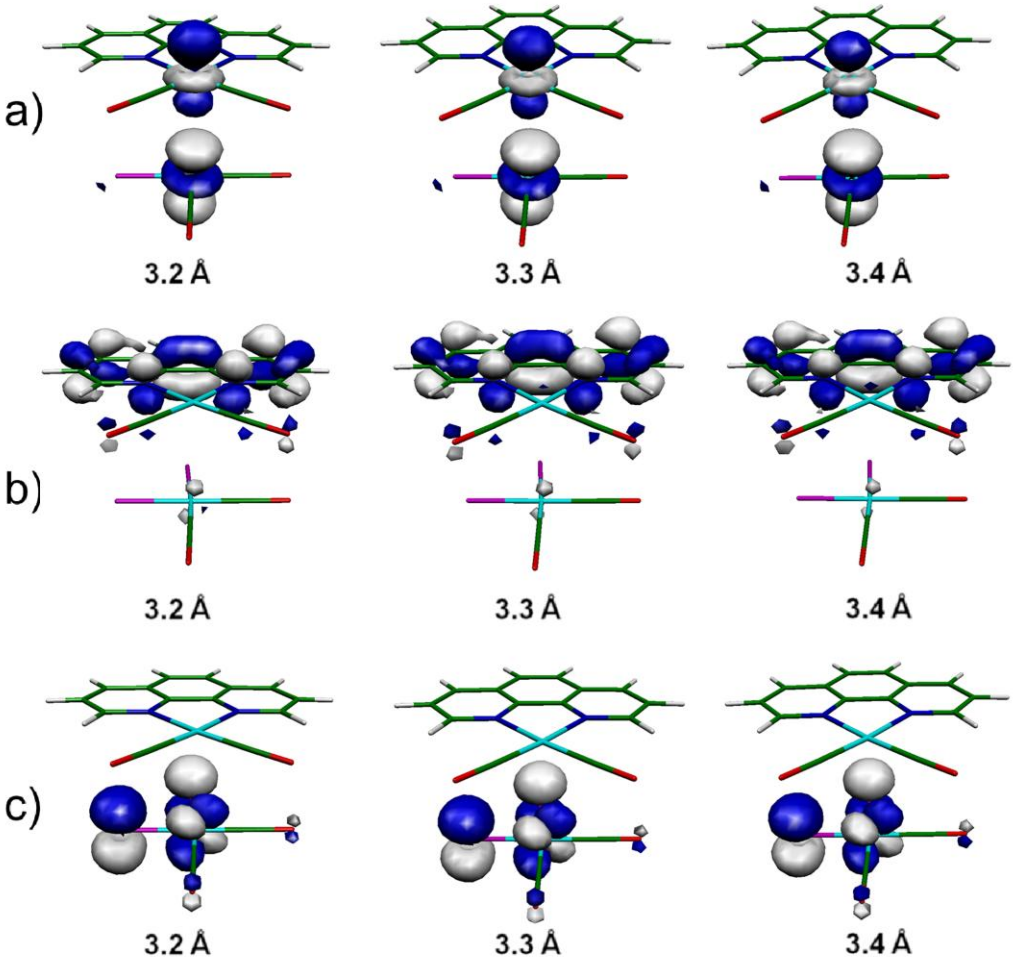

Figure S3. The HOMO (a), LUMO (b) and HOMO-1 (c) orbitals of [Rh(1,10-phen)$(CO)_2$][Rh$(CO)_2Cl_2$] (**1**) system at different rhodium···rhodium distance.

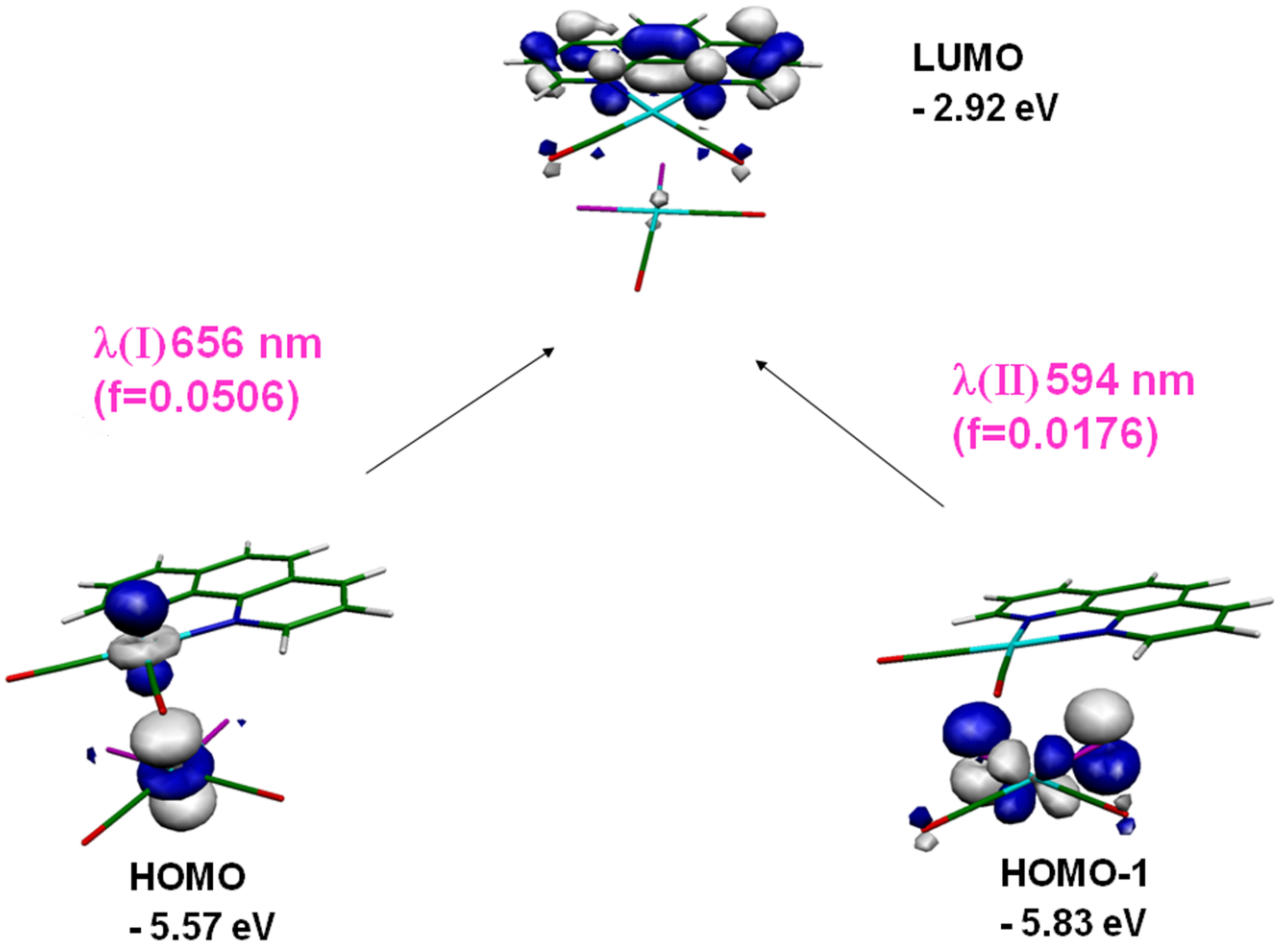

Figure S4. The origin of the absorption signals **I** and **II** for [Rh(1,10-phen)$(CO)_2$][Rh$(CO)_2Cl_2$] (**2**) at the Rh···Rh distance of 3.3 Å.

Table S3. The contribution of the Rh and the ligand orbitals to the frontier orbitals of **1** and **2** at different Rh···Rh distances.

Complex 1	3.2 Å			3.3 Å			3.4 Å		
	HOMO-1	HOMO	LUMO	HOMO-1	HOMO	LUMO	HOMO-1	HOMO	LUMO
Rh1	0.3	**29**	5	0.2	**24**	5	0.1	**19**	5
Rh2	**35**	**60**	5	**35**	**65**	5	**36**	**71**	4
bpy	2	3	**82**	1	3	**83**	1	2	**83**
CO1	0.2	2	6	0.2	2	6	0.2	2	6
CO2	5	1	0.5	5	1	0.4	5	1	0.3
Cl	**58**	5	1	**58**	5	1	**58**	5	1

Complex 2	3.2 Å			3.3 Å			3.4 Å		
	HOMO-1	HOMO	LUMO	HOMO-1	HOMO	LUMO	HOMO-1	HOMO	LUMO
Rh1	0.3	**29**	5	0.2	**24**	5	0.1	**19**	5
Rh2	**33**	**61**	6	**34**	**66**	5	**34**	**72**	5
phen	2	3	**82**	2	3	**83**	2	2	**83**
CO1	0.2	2	6	0.2	2	6	0.1	2	6
CO2	5	1	0.5	5	1	0.4	5	1	0.3
Cl	**59**	5	1	**59**	4	1	**59**	4	1

Experimental

Materials

The $RhCl_3$ hydrate (Rh 38.5 – 45.5%) was purchased from Alfa Aesar. 2,2'-bipyridine and 1,10-phenanthroline were produced by Aldrich and Acros, respectively. The ethanol (99.5%) was manufactured by Primalco. The carbon monoxide (98%) was produced by AGA.

Experimental methods

The elemental content was determined by Vario MICRO V1.7.0 CHNS Mode and acetanilide was used as the standard. The FTIR spectra measurements were performed using a Nicolet Magna IR Spectrometer 750.

Synthesis of complex $[Rh(CO)_2(2,2'\text{-bpy})][RhCl_2(CO)_2]$ (1)

The rhodium trichloride (100 mg, 0.48 mmol) and 2,2'-bibyridine (37 mg, 0.24 mmol) were placed in a Berghof autoclave in a PTF liner and methanol (4 ml) was added. The autoclave was pressurized with 50 bar of carbon monoxide. The reaction temperature was 125°C and the reaction time was 6 days. The autoclave was allowed to cool down in the oven for 5h. The metallic reddish needle crystals (**1**) were filtrated. The crystals were separated under microscope and analyzed (30 mg, 23%). (Found: C, 30.90; H, 1.50; N, 5.06, Calcd. for $\{[Rh(CO)_2(2,2'\text{-bpy})][RhCl_2(CO)_2]\}$ C, 30.86; H, 1.48; N, 5.14. ν_{max}(KBr)/cm^{-1} 2092 (CO), 2065 (CO), 2029(CO), 1988(CO). Crystals suitable for X-ray analysis were crystallized from ethanol solution.

Synthesis of complex 2 (and 3)

The rhodium trichloride (100 mg, 0.48 mmol) and 1,10-phenanthroline (43 mg, 0.24 mmol) were placed in a Berghof autoclave in a PTF liner and methanol (4 ml) was added. The autoclave was pressurized with 50 bar of carbon monoxide. The reaction temperature was 125°C and the reaction time was 20 hours. The autoclave was allowed to cool down in the oven for 2h and 2 hours in ice bath. In addition to metallic blackish needles of 2, a minor yellow crystalline product (a few crystals) of $[RhCl_2(1,10\text{-phen})_2][Rh(CO)_2Cl_2]$ (**3**) was formed. The metallic blackish needles (**2**) were filtrated. The crystals were used without further purification. (76 mg, 56%). (Found: C, 33.59; H, 1.65; N, 4.86. Calcd. for $\{[Rh(CO)_2(1,10\text{-phen})][RhCl_2(CO)_2]\}$ C, 33.78; H, 1.42; N, 4.92. ν_{max}(KBr)/cm^{-1} 2097 (CO), 2086 (CO), 2058 (CO), 2037(CO), 2016 (CO), 1993(CO), 1980 (CO). The minor side product **3** was analysed only by single-crystal X-ray diffraction. Crystals suitable for X-ray analysis were crystallized from ethanol solution.

X-ray Crystal Structure Determination

The crystals of **1-3** were immersed in cryo-oil, mounted in a Nylon loop, and measured at a temperature of 100K. The X-ray diffraction data were collected on a Bruker Kappa Apex II diffractometer using Mo Kα radiation (λ = 0.71073 Å). The *Apex2*[S1] program package was used for cell refinements and data reductions. The structures were solved by direct method using or *SHELXS-97*[S2] programs with a *WinGX*[S3] graphical user interface. A semi-empirical or numerical absorption (*SADABS*)[S4] was applied to all of the data. Structural refinements were carried out using *SHELXL-97*.[S2] The structure of complex **1** was refined as a racemic twin in a non-centrosymmetrical space group I-4. The BASF value was refined to 0.5871. The hydrogen atoms were positioned geometrically and constrained to ride on their parent atoms, with C-H = 0.95 Å. U_{iso} = 1.2 U_{eq} (parent atom). The crystallographic details for complexes **1-3** are summarized in Table S4 and selected bond lengths and angles in Table S5. CCDC-871906 (**1**), -871907 (**2**) and -871908 (**3**) contain the supplementary crystallographic data for this paper. These data can be obtained free of charge from The Cambridge Crystallographic Data Center via www.ccdc.cam.ac.uk/data_request/cif.

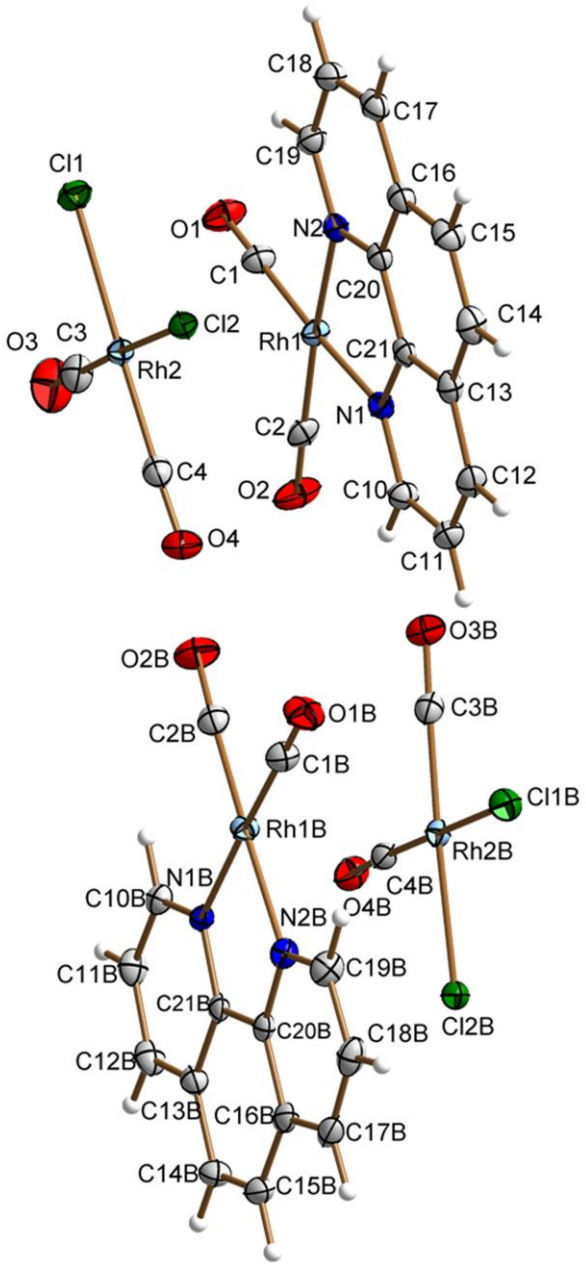

Figure S6. The thermal ellipsoid plot of [Rh(1,10-phen)$(CO)_2$][$RhCl_2(CO)_2$] **2** at 50% probability level at 100 K.

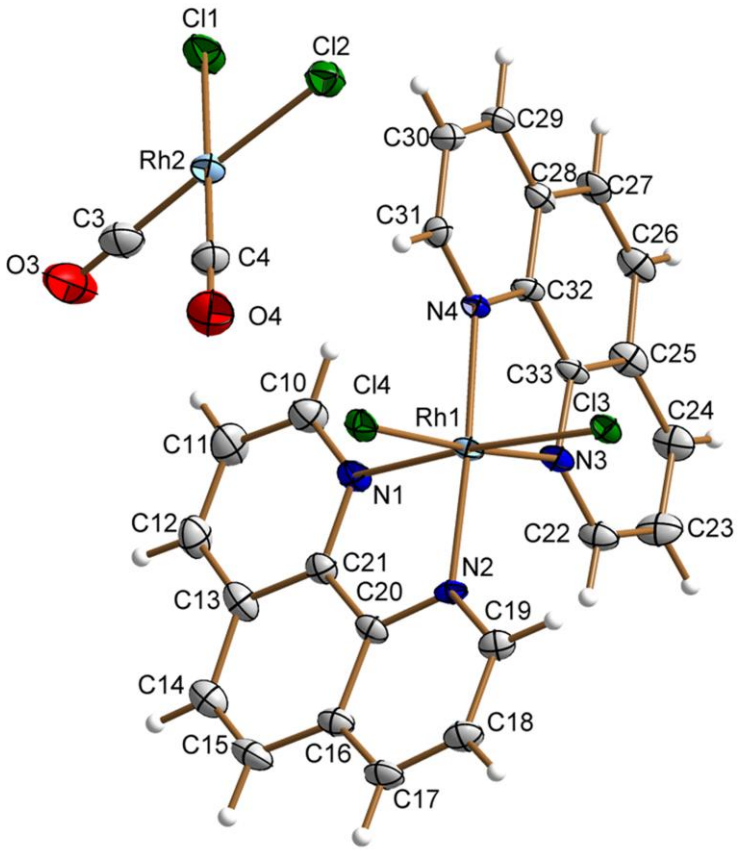

Figure S7. The thermal ellipsoid plot of $[Rh(1,10\text{-phen})_2Cl_2][RhCl_2(CO)_2]$ **3** at 50% probability level.

Table S4. Crystal data of **1-3**.

	1	**2**	**3**
empirical formula	$C_{14}H_8Cl_2N_2O_4Rh_2$	$C_{16}H_8Cl_2N_2O_4Rh_2$	$C_{26}H_{16}Cl_4N_4O_2Rh_2$
Fw	544.94	568.96	764.05
temp (K)	100(2)	100(2)	100(2)
λ(Å)	0.71073	0.71073	0.71073
cryst syst	Tetragonal	Triclinic	Triclinic
space group	I $\bar{4}$	P $\bar{1}$	P $\bar{1}$
a (Å)	22.1438(8)	6.56520(10)	8.7104(11)
b (Å)	22.1438(8)	16.7058(4)	11.2066(14)
c (Å)	6.7080(3)	16.9994(4)	14.5161(19)
α (deg)	90	72.6080(10)	96.101(3)
β (deg)	90	80.9340(10)	90.288(3)
γ(deg)	90	86.5110(10)	107.315(2)
V (Å^3)	3289.3(2)	1756.79(6)	1344.1(3)
Z	8	4	2
ρ_{calc} (Mg/m^3)	2.201	2.151	1.888
μ(Mo Kα) (mm^{-1})	2.352	2.207	1.658
No. reflns.	9669	15324	12064
Unique reflns.	3785	10077	6107
Goof	1.042	1.014	1.041
R_{int}	0.0310	0.0193	0.0408
R1[a] ($I \geq 2\sigma$)	0.0247	0.0269	0.0382
wR2[b] ($I \geq 2\sigma$)	0.0507	0.0508	0.0847

[a] $R1 = \Sigma||F_o| - |F_c||/\Sigma|F_o|$. [b] $wR2 = [\Sigma[w(F_o^2 - F_c^2)^2]/\Sigma[w(F_o^2)^2]]^{1/2}$.

Table S5. Selected bond distances (Å) and angles (°) for compounds **1-3**.

	1	**2**	**3**
Rh(1)-N(1)	2.077(3)	2.078(2)	2.027(3)
Rh(1)-N(2)	2.070(3)	2.078(2)	2.046(3)
Rh(1)-N(3)			2.038(3)
Rh(1)-N(4)			2.037(3)
Rh(1B)-N(1B)		2.076(2)	
Rh(1B)-N(2B)		2.080(2)	
Rh(1)···Rh(2)	3.3174(5)	3.3155(3)	
Rh(1)···Rh(2)#1	3.4116(5)		
Rh(1)···Rh(2)#2		3.2734(3)	
Rh(1B)···Rh(2B)		3.3211(3)	
Rh(1B)···Rh(2B)#3		3.3498(3)	
N(1)-Rh(1)-N(2)	78.65(11)	80.10(8)	81.08(12)
N(3)-Rh(1)-N(4)			81.62(12)
N(1B)-Rh(1B)-N(2B)		79.94(8)	
Rh(2)···Rh(1)···Rh(2)#1	170.927(11)		
Rh(2)···Rh(1)···Rh(2)#2		170.275	
Rh(2B)···Rh(1B)···Rh(2B)#3		159.573	
dihedral angle	4.201(128)		
angle between the square planar planes (N-N-Rh-C-C, Cl-Cl-Rh-C-C)	3.816(90)	0.345(56), 0.740(42)	

Symmetry transformations used to generate equivalent atoms: #1 x,y,z+1; #2 x-1,y,z; #3 x+1,y,z

Computational details

The DFT calculations were carried out with Gaussian03 program package[S5] using PBE1PBE[S6] density functional. Huzinaga's all electron basis set[S7] with extra p-polarization function was used for Rh and standard all electron basis set 6-31G(d) for Cl, C, O, N and H. The model compound for the DFT calculations contained a cation-anion pair of $[Rh(L)(CO)_2][Rh(CO)_2Cl_2]$ (Scheme SI). The dinuclear models with one $[Rh(L)(CO)_2]^+$ and $[Rh(CO)_2Cl_2]^-$ unit were obtained from X-ray data with no further optimization. The time-dependent DFT was used to study excitations and to generate UV-VIS spectra in vacuum with different Rh-Rh distance. The wavefuctions for the charge density analysis were calculatated by using a tetranuclear units (two cation-anion pairs, Scheme SI) extracted from the experimental structures.

Charge density analysis

The charge density analysis was carried out by AIM2000[S9] using the wavefunctions created by the DFT calculations. The calculations were performed using tetranuclear moieties with two $[Rh(L)(CO)_2][Rh(CO)_2Cl_2]$ pairs. The results also were compared with the previously reported stacks of cationic $[Rh(H_2bim)(CO)_2]^+$ complexes with NO_3^- as the counter anion.[S10] The results are summarized in Table S6. For both structures **1** and **2** the bond critical points were found between all adjacent Rh atoms in the chains. The electron densities at the critical points vary between 0.102 to 0.128 $eÅ^{-3}$, which is well in line with the corresponding values in the cationic stack of $[Rh(H_2bim)(CO)_2]^+$ with slightly shorter Rh-Rh distance. As a comparison, the electron densities of a metal-metal bond in a covalent $[Ru(CO)_4]_n$ chain is about 0.3 $eÅ^{-3}$.[S10] The kinetic energy/potential energy ratio ([V]/G) is between 1 and 2, which is indicative for electrostatic interactions with some covalent contribution.[S9] In addition AIMAll[S11] was used to calculate the electron delocalization indices that can be used to describe the nature of metal…metal interactions.[S12]

Table S6. Properties of the electron density at the bond critical points of Rh···Rh .

Structure	Rh···Rh [Å]	e-density e Å^{-3}	laplacian e Å^{-5}	|λ1|/λ3, elliptisyys -	G, Kinetic energy hartree	V,potential energy hartree	H, energy hartree	|V|/G -	δ(ΩRh-ΩRh)
1 a	3.31775	0.1168	0.7263	0.2016	0.0101	-0.0127	-0.0026	1.2546	0.165
1 b	3.41145	0.1023	0.6767	0.1963	0.0087	-0.0104	-0.0017	1.1930	0.136
2 a	3.31584	0.1218	0.7255	0.1846	0.0103	-0.0130	-0.0027	1.2675	0.177
2 b	3.27299	0.1280	0.7572	0.2078	0.0111	-0.0143	-0.0032	1.2893	0.181
2B a*	3.32119	0.1155	0.7153	0.2032	0.0100	-0.0125	-0.0025	1.2551	0.168
2B b*	3.34973	0.1128	0.7348	0.2017	0.0098	-0.0120	-0.0022	1.2248	0.145
$[Rh(H_2bim)(CO)_2][NO_3]$**	3.23795	0.1380	0.8089	0.2123	0.0121	-0.0158	-0.0037	1.3070	0.197

*The structure **2** contained two independend chains (see the figure S6).
**The results are obtained from the reference S8 (experimental structure at 100 K).
for a and b see Scheme SI

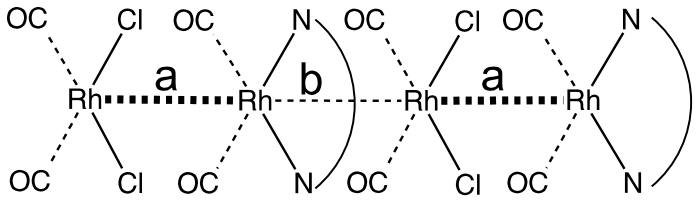

Scheme S1. Schematic representation of the tetranuclear molecular model with the two Rh···Rh distances used for charge density analysis.

References

S1 Bruker AXS, *APEX2 - Software Suite for Crystallographic Programs -,* Bruker AXS, Inc.: Madison, WI, USA, 2009.

S2 Sheldrick, G. M. *Acta Cryst.* 2008, **A64**, 112-122.

S3 Farrugia, L. J. *J. Appl Cryst.* 1999, **32,** 837-838.

S4 Sheldrick, G. M. *SADABS - Bruker Nonius scaling and absorption correction -,* Bruker AXS, Inc.: Madison, Wisconsin, USA, 2008.

S5 Frisch, M. J.; Trucks, G. W.; Schlegel, H. B.; Scuseria, G. E.; Robb, M. A.; Cheeseman, J. R.; Montgomery Jr., J. A.; Vreven, T.; Kudin, K. N.; Burant, J. C.; Millam, J. M.; Iyengar, S. S.; Tomasi, J.; Barone, V.; Mennucci, B.; Cossi, M.; Scalmani, G.; Rega, N.; Petersson, G. A.. Nakatsuji, H.; Hada, M.; Ehara, M.; Toyota, K.; Fukuda, R.; Hasegawa, J.; Ishida, M.; Nakajima, T.; Honda, Y.; Kitao, O.; Nakai, H.; Klene, M.; Li, X.; Knox, J. E.; Hratchian, H. P.; Cross, J. B.; Adamo, C.; Jaramillo, J.; Gomperts, R.; Stratmann, R. E.; Yazyev, O.; Austin, A. J.; Cammi, R.; Pomelli, C.; Ochterski, J. W.; Ayala, P. Y.; Morokuma, K.; Voth, G. A.; Salvador, P.; Dannenberg, J. J.; Zakrzewski, V. G.; Dapprich, S.; Daniels, A. D.; Strain, M. C.; Farkas, O.; Malick, D. K.; Rabuck, A. D.; Raghavachari, K.; Foresman, J. B.; Ortiz, J. V.; Cui, Q.; Baboul, A. G.; Clifford, S.; Cioslowski, J.; Stefanov, B. B.; Liu, G.; Liashenko, A.; Piskorz, P.; Komaromi, I.; Martin, R. L.; Fox, D. J.; Keith, T.; Al-Laham, M. A.; Peng, C. Y.; Nanayakkara, A.; Challacombe, M.; Gill, P. M. W.; Johnson, B.; Chen, W.; Wong, M. W.; Gonzalez, C.; Pople J, A. Gaussian 03, Revision C.02, Gaussian, Inc., Wallingford CT, 2004.

S6 Perdew, J. P.; Burke, K.; Ernzerhof, M. *Phys. Rev. Lett.* 1996, **77**, 3865-3868.

S7 Huzinaga, S. (Ed.); Andzelm, J.; Klobukowski, M.; Radzio-Andzelm, E.; Sakai, Y.; Tatewaki, H. in *Gaussian Basis Sets for Molecular Calculations*; Elsevier, Amsterdam, 1984.

S8 Laurila, E.; Oresmaa, L.; Hirva, P.; Haukka, M. *Crystal Growth & Design* **2010**, *10*, 3775-3786.

S9 AIM2000 (Version 2.0), Biegler-König, F.; Schönbohm, J. 2002.

S10 Niskanen, M.; Hirva, P.; Haukka, M. *J. Chem. Theory. Comput.* **2009**, *5*, 1084-1090.

S11 AIMAll (Version 12.09.23), Todd A. Keith, TK Gristmill Software, Overland Park KS, USA, 2012

S12 Farrugia, L. J.; Macchi, P. *Struct. Bond*. **2012**, *146*, 127-158.